

REVISITING THE COMPLETENESS AND THE LUMINOSITY FUNCTION IN HIGH-REDSHIFT  
LOW-LUMINOSITY QUASAR SURVEYSMANA NIIDA<sup>1</sup>, TOHRU NAGAO<sup>2</sup>, HIROYUKI IKEDA<sup>3</sup>, KENTA MATSUOKA<sup>4</sup>,  
MASAKAZU A. R. KOBAYASHI<sup>5</sup>, YOSHIKI TOBA<sup>2,6</sup>, AND YOSHIKI TANIGUCHI<sup>7</sup>*Draft version March 5, 2024*

## ABSTRACT

Recent studies have derived quasar luminosity functions (QLFs) at various redshifts. However, the faint side of the QLF at high redshifts is still too uncertain. An accurate estimate of the survey completeness is essential to derive an accurate QLF for use in studying the luminosity-dependent density evolution of the quasar population. Here we investigate how the luminosity dependence of quasar spectra (the Baldwin effect) and the attenuation model for the inter-galactic medium (IGM) affect the completeness estimates. For this purpose, we revisit the completeness of quasar surveys specifically at  $z \sim 4 - 5$ , using the COSMOS images observed with Subaru/Suprime-Cam. As the result, we find that the completeness estimates are sensitive to the luminosity dependence of the quasar spectrum and difference in the IGM attenuation models. At  $z \sim 4$ , the number density of quasars when we adopt the latest IGM model and take the luminosity dependence of spectra into account are  $(3.49 \pm 1.62) \times 10^{-7} \text{ Mpc}^{-3} \text{ mag}^{-1}$  for  $-24.09 < M_{1450} < -23.09$  and  $(5.24 \pm 2.13) \times 10^{-7} \text{ Mpc}^{-3} \text{ mag}^{-1}$  for  $-23.09 < M_{1450} < -22.09$ , respectively, which are  $\sim 24\%$  lower than that estimated by the conventional method. On the other hand, at  $z \sim 5$ , a  $1\sigma$  confidence upper limit of the number density at  $-24.5 < M_{1450} < -22.5$  in our new estimates is  $\sim 43\%$  higher than that estimated previously. The results suggest that the luminosity dependence of the quasar spectrum and the IGM model are important for deriving accurate number density of high- $z$  quasars. Even taking these effects into account, the inferred luminosity-dependent density evolution of quasars is consistent with the AGN down-sizing evolutionary picture.

*Subject headings:* galaxies: active — galaxies: luminosity function, mass function — quasars: emission lines — quasars: general

## 1. INTRODUCTION

It is now widely recognized that the huge radiative energy released from active galactic nuclei (AGNs) is powered by the gravitational energy of supermassive black holes (SMBHs) at the center of AGNs (e.g., Rees 1984). The mass of SMBHs ( $M_{\text{BH}}$ ) in quasars, that belong to the most luminous class of AGNs, reaches up to  $\sim 10^9 M_{\odot}$  or even more (e.g., Willott et al. 2010; Shen & Kelly 2012). Interestingly, such massive SMBHs are seen even at very high redshifts,  $z \sim 6 - 7$  (e.g., Kurk et al. 2007; Mortlock et al. 2011; Venemans et al. 2013, 2015; Wu et al. 2015). However, it is totally unclear when and how those SMBHs have formed and evolved. On the other hand, it has been observationally reported that there is a tight correlation between the mass of the host bulges ( $M_{\text{bulge}}$ ) and  $M_{\text{BH}}$  (e.g., Marconi & Hunt 2003;

Häring & Rix 2004; Gültekin et al. 2009). This correlation suggests that the SMBHs and their host galaxies have evolved with the close interplay, that is now recognized as the galaxy-SMBH coevolution. Therefore the observational study on the redshift evolution of SMBHs is important also for understanding the total picture of the galaxy evolution, not only for understanding the evolution of SMBHs themselves.

For exploring the cosmological evolution of SMBHs observationally, one important class of AGNs is the quasar. This is because (i) quasars are in the phase where SMBHs are acquiring their mass via the gas accretion very actively and (ii) the huge luminosity of quasars enables us to measure  $M_{\text{BH}}$  through spectroscopic observations, even in the very distant Universe. Even without spectra, a very rough guess of  $M_{\text{BH}}$  can be obtained through their luminosity by assuming a certain Eddington ratio. In this sense, it is very interesting to investigate the number density evolution of quasars as a function of the redshift and luminosity; i.e., the redshift evolution of the quasar luminosity function (QLF). In other words, the accurate measurement of the QLF at a wide redshift range is a promising approach to study the cosmological evolution of SMBHs.

The QLF at  $z \lesssim 3$  has been extensively measured over a wide luminosity range (e.g., Siana et al. 2008; Croom et al. 2009; Ross et al. 2013; Palanque-Delabrouille et al. 2013), and accordingly it is recognized that the QLF is expressed by the broken power-law formula. Though the brighter part of the

niida@cosmos.phys.sci.ehime-u.ac.jp

<sup>1</sup> Graduate School of Science and Engineering, Ehime University, Bunkyo-cho 2-5, Matsuyama 790-8577, Japan<sup>2</sup> Research Center for Space and Cosmic Evolution, Ehime University, Bunkyo-cho 2-5, Matsuyama 790-8577, Japan<sup>3</sup> National Astronomical Observatory of Japan, Mitaka, Tokyo 181-8588, Japan<sup>4</sup> Department of Astronomy, Kyoto University, Kitashirakawa-Oiwake-cho, Sakyo-ku, Kyoto 606-8502, Japan<sup>5</sup> Faculty of Natural Sciences, National Institute of Technology, Kure College, 2-2-11, Agaminami, Kure, Hiroshima 737-8506, Japan<sup>6</sup> Academia Sinica Institute of Astronomy and Astrophysics, PO Box 23-141, Taipei 10617, Taiwan<sup>7</sup> The Open University of Japan, 2-11, Wakaba, Mihama-ku, Chiba 261-8586, Japan

QLF at  $z \gtrsim 4$  has been also measured (Richards et al. 2006; Shen & Kelly 2012), the faint side of the QLF is still controversial (e.g., Glikman et al. 2010, 2011; Ikeda et al. 2011, 2012; Masters et al. 2012). Once focusing on high-luminosity quasars, previous observations suggest that the number density of luminous quasars increased from the early Universe to  $z \sim 2$  and then decreased to the current Universe (e.g., Richards et al. 2006; Croom et al. 2009). It is more interesting to study possible luminosity dependences of the quasar number-density evolution (luminosity-dependent density evolution; LDDE). Recent optical surveys of high-redshift quasars have reported that lower-luminosity quasars show the peak of the number density at lower redshifts than higher-luminosity quasars (e.g., Croom et al. 2009; Ikeda et al. 2011, 2012). Since the quasar luminosity at a given Eddington ratio corresponds to  $M_{\text{BH}}$ , the reported LDDE trend is that is sometimes called the down-sizing evolution. Such a down-sizing trend has been reported also by some X-ray surveys (e.g., Ueda et al. 2003, 2014; Hasinger et al. 2005; Miyaji et al. 2015; see also Enoki et al. 2014 and references therein for theoretical works on the AGN down-sizing evolution). Note that the down-sizing evolution has been originally discussed for explaining the redshift evolution of the galaxy number density and mass function (e.g., Cowie et al. 1996; Neistein et al. 2006; Fontanot et al. 2009). Therefore the observational study on the AGN down-sizing evolution is exciting also for exploring the galaxy-SMBH co-evolution.

One caveat in the previous study on the AGN down-sizing evolution is that the number density of low-luminosity quasars at high redshifts is quite uncertain, that prevents us from understanding the total picture of the quasar LDDE. Ueda et al. (2014) mentioned that the number ratio of low-luminosity quasars to high-luminosity quasars is possibly higher at  $z > 3$  (“up-down sizing”; see also Glikman et al. 2010, 2011), but such detailed studies on the quasar LDDE at high redshifts required more statistically reliable QLFs with a wide luminosity range. Here we point out two issues that may introduce large systematic errors in the previous QLF studies. One is the effect of the luminosity dependence of quasar spectra on the completeness in quasar surveys. The survey completeness is usually estimated by adopting a typical template of the quasar spectrum, constructed empirically (e.g., Vanden Berk et al. 2001) or based on simple models (e.g., Ikeda et al. 2011, 2012). However the equivalent width ( $EW$ ) of broad emission lines in the quasar spectrum strongly depends on the quasar luminosity, in the sense that lower-luminosity quasars show emission lines with a larger  $EW$  (the Baldwin effect; Baldwin 1977; Kinney et al. 1990; Baskin & Laor 2004; see also Nagao et al. 2006 and references therein for the luminosity dependence of flux ratios of quasar broad lines). If the quasar luminosity investigated in a survey is much lower than that used for the template in the completeness, the quasar colors calculated from the template may be systematically different from the actual quasar colors due to the unexpected contribution of emission-line fluxes into broad-band magnitudes. Therefore it is essential to know how the Baldwin effect affects the completeness in quasar surveys and the resultant QLFs. Another possible source of system-

atic errors in the QLF study is the inter-galactic medium (IGM) attenuation by neutral hydrogen, that is also important in the completeness estimate because the color of high-redshift quasars is sensitive to the IGM absorption. Recently Inoue et al. (2014) pointed out that the previous models of the IGM attenuation (such as the model by Madau 1995) tend to overestimate the optical depth of the IGM. Thus it is important to examine how the derived QLF is different from the previous estimate when we adopt the recent IGM model by Inoue et al. (2014) that is more consistent with recent observational data of quasar absorption-line systems.

In this paper, we investigate how the Baldwin effect and the IGM models affect the quasar colors, completeness estimates, and the resultant QLFs, specifically focusing on quasars at  $z \sim 4 - 5$ . Based on the obtained results, we revisit the redshift evolution of the quasar space density in a wide luminosity range to examine the quasar LDDE. This paper is organized as follow. In Section 2, we describe how the quasar color is affected by the Baldwin effect and the adopted IGM model. In Section 3 and Section 4, we show the resultant survey completeness and the QLF for  $z \sim 4$  and 5. Finally we present the summary of this paper in Section 5. Throughout this paper, we adopt a  $\Lambda$ CDM cosmology with  $\Omega_m = 0.3$ ,  $\Omega_\Lambda = 0.7$ , and the Hubble constant of  $H_0 = 70 \text{ km s}^{-1} \text{ Mpc}^{-1}$ .

## 2. DATA

### 2.1. BOSS Quasars

For examining how the Baldwin effect affects the quasar colors, the  $EW$  of emission lines should be known as a function of the quasar luminosity. To measure the  $EW$ , we focus on the archival data of the Baryon Oscillation Spectroscopic Survey (BOSS; Dawson et al. 2013) and investigate the spectra of quasars in the BOSS quasar catalog (Pâris et al. 2012) in the Data Release 9 (DR9; Ahn et al. 2012) of the Sloan Digital Sky Survey (SDSS; York et al. 2000). In the BOSS observations, two double-armed spectrographs, which are upgraded and cover a wider spectral range than those used by the former SDSS observations, are used (Smee et al. 2013). Furthermore the BOSS targeted quasars with  $\sim 2$  magnitudes fainter than the original SDSS spectroscopic targets, i.e.,  $g^* < 22$  or  $i^* < 21$  (Pâris et al. 2012). This wide magnitude range of the quasar sample is useful for our analysis of the Baldwin effect. The spectral resolution varies from  $R \sim 1,300$  at  $3600 \text{ \AA}$  to  $\sim 2,500$  at  $10000 \text{ \AA}$  (Smee et al. 2013). This resolution is enough for our analysis, since the broad emission lines in quasars have a large velocity width typically ( $> 1,000 \text{ km s}^{-1}$ ).

The total area covered by the DR9 is  $3,275 \text{ deg}^2$ , in which 87,822 spectroscopically confirmed quasars are identified (Pâris et al. 2012). In order to cover most strong rest-frame UV emission lines such as  $\text{Ly}\alpha$  and  $\text{C IV}$ , we specifically focus on the redshift range of  $2 \leq z < 5$  where 65,419 quasars are listed in the catalog of Pâris et al. (2012). Among them, quasars showing broad absorption-line (BAL) features in their spectra (6,449 objects, that are identified through the **BAL\_FLAG** parameter in the catalog of Pâris et al. 2012) are removed because we cannot measure the  $EW$  correctly in those cases. Then we select objects whose redshift is accurately measured, by adopting the criteria of **ZWARNING** flag = 0 and

$\text{ERR\_ZPIPE} \leq 0.001$  (52,290 objects). An additional criterion is also adopted for avoiding the mis-identification of emission lines (and consequently the wrong redshift), by comparing the redshift measured through the SDSS pipeline (Z\_PIPE) and that measured through the visual inspection (Z\_VI). In this step, 161 objects satisfying  $|\text{Z\_VI} - \text{Z\_PIPE}| > 0.05$  are removed. For selecting quasars with a spectrum which has a high signal-to-noise ratio, we adopt another criterion of  $\text{SNR\_SPEC} > 1$  (43,962 objects). Then we selected 43,956 objects whose luminosity is in the range of  $-31 \leq M_i[z = 2] < -23$ , where  $M_i[z = 2]$  is the  $K$ -corrected  $i$ -band magnitude at  $z = 2$  (see Richards et al. 2006; Ross et al. 2013), because in this luminosity range there are enough number of quasars for each luminosity. Finally, we remove three quasars whose FITS header has a problem. The number of finally selected BOSS quasars in our analysis is 43,953.

## 2.2. Composite Spectra of BOSS Quasars

To investigate the relation between the quasar luminosity and  $EW$  of broad emission lines in the quasar spectrum statistically, we analyze composite spectra of BOSS quasars for each luminosity. This stacking analysis is a powerful method for studying the luminosity dependence of quasar spectral features, since it minimizes the dispersion of spectral features in quasar spectra in each luminosity bin. Another advantage of the stacking analysis is measuring the spectral features of low-luminosity quasars whose individual spectra show very faint spectral features with very low signal-to-noise ratios (see, e.g., Vanden Berk et al. 2001; Nagao et al. 2006).

First, we confirm that  $EW_{\text{rest}}(\text{C IV})$  of BOSS quasars does not depend on redshift, that is consistent with earlier works (e.g., Dietrich et al. 2002; Croom et al. 2002, see Appendix). Therefore we combine the spectra of quasars in the whole redshift range of  $2 \leq z < 5$  to make the composite spectra as a function of the absolute magnitude. This enables us to examine the luminosity dependence in a wide luminosity range, because quasars at higher redshift and those at lower redshift trace the higher luminosity and lower luminosity ranges, respectively. We divide the absolute magnitude range of  $-31 \leq M_i[z = 2] < -23$  into 8 magnitude bins with the bin width of  $\Delta M_i[z = 2] = 1$  (see Table 1), through the following analysis.

We then convert each spectrum from the observed frame to the rest frame, and then normalize the each converted spectrum by averaging the flux at  $1445 \text{ \AA} < \lambda_{\text{rest}} < 1485 \text{ \AA}$ , which contains few emission-lines contributions (see, e.g., Vanden Berk et al. 2001; Nagao et al. 2006). Then we make the composite spectra for each absolute magnitude bin by using the IRAF `scombine` task in the `noao.onedspec` package. The number of quasars used to make the composite spectrum for each absolute magnitude is given in Table 1. In this stacking process, we adopt the  $3\sigma$  clipping for removing the outlier pixels and then calculate the average flux at each wavelength in the logarithmic scale. Figure 1 shows the obtained composite spectra for each absolute magnitude in the rest frame.

Figure 1 clearly shows a systematic trend that lower-luminosity quasars tend to show emission lines with a larger  $EW$ . This is consistent with previous works

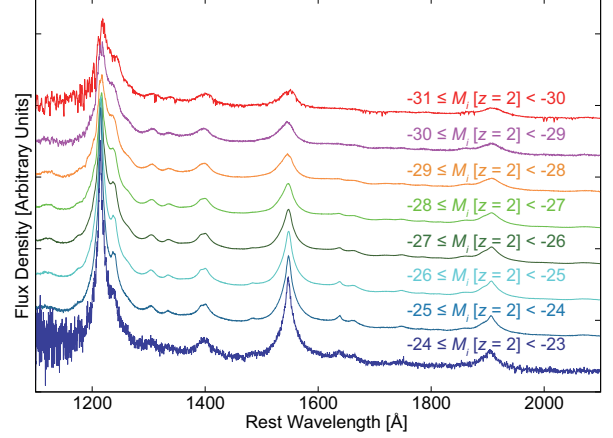


FIG. 1.— The composite spectra of BOSS quasars for each absolute magnitude. The difference of the line color denotes the difference of the luminosity. For clarifying the difference of each composite spectrum in the figure, we shift each composite spectrum toward the vertical direction.

TABLE 1  
THE MEASURED  $EW_{\text{rest}}(\text{C IV})$  OF COMPOSITE SPECTRA OF BOSS QUASARS

$M_i[z = 2]$ [mag]	$EW_{\text{rest}}(\text{C IV})$ [Å]	$\sigma(EW_{\text{rest}}(\text{C IV}))$ [Å]	$N^a$
$-31 \leq M_i < -30$	17.7	6.67	5
$-30 \leq M_i < -29$	21.2	10.8	84
$-29 \leq M_i < -28$	23.8	11.1	1,047
$-28 \leq M_i < -27$	27.6	13.6	5,479
$-27 \leq M_i < -26$	33.5	18.0	14,424
$-26 \leq M_i < -25$	42.3	23.2	17,719
$-25 \leq M_i < -24$	49.3	24.5	5,131
$-24 \leq M_i < -23$	59.5	34.8	64

<sup>a</sup> Number of quasars in each magnitude bin.

of the stacking analysis of high-redshift quasars (e.g., Nagao et al. 2006; Matsuoka et al. 2011). To investigate this trend quantitatively, we measure  $EW(\text{C IV})$  for each composite spectrum by adopting the method of Vanden Berk et al. (2001). For subtracting the continuum flux, we define the local continuum around the C IV emission. This local continuum is defined by the median flux densities in the two wavelength regions,  $1460 \text{ \AA} < \lambda_{\text{rest}} < 1475 \text{ \AA}$  and  $1600 \text{ \AA} < \lambda_{\text{rest}} < 1630 \text{ \AA}$ . Then we measure the flux of the C IV emission and the underlying continuum emission, that is converted to  $EW_{\text{rest}}(\text{C IV})$ . We also derive the standard deviation of  $EW_{\text{rest}}(\text{C IV})$  for each absolute magnitude bin, by calculating the distribution of  $EW_{\text{rest}}(\text{C IV})$  in the individual (i.e., pre-stacking) spectrum of the BOSS quasars. The measurement results are given in Table 1. We show the measured  $EW_{\text{rest}}(\text{C IV})$  as a function of the absolute magnitude of quasars in Figure 2. A clear correlation between the  $EW_{\text{rest}}(\text{C IV})$  and the absolute magnitude is seen, that is consistent with the Baldwin effect. We apply the weighted least-squares fit to the  $EW_{\text{rest}}(\text{C IV})$ , adopting the following linear function:

$$\log[EW_{\text{rest}}(\text{C IV})] = A \times M_i[z = 2] + B, \quad (1)$$

where A and B are fitting parameters. The fitting results tell us  $A = 0.074^{+0.003}_{-0.002}$  and  $B = 3.503^{+0.067}_{-0.096}$ . The fitting result is shown with the dashed line in Figure 2.



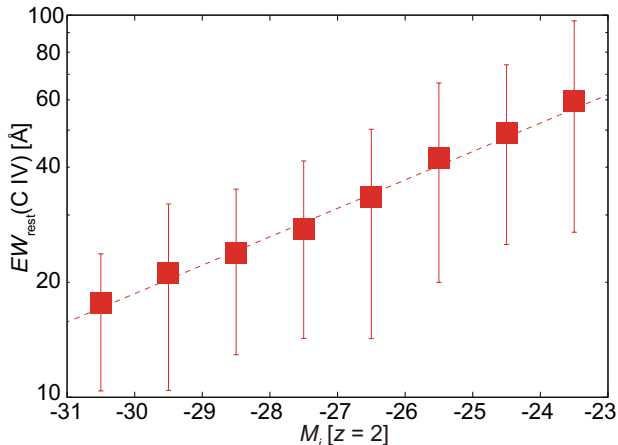


FIG. 2.— The correlation between  $EW_{\text{rest}}(\text{C IV})$  measured from composite spectra of BOSS quasars and their absolute magnitude. The  $1\sigma$  error bars show the standard deviation of  $EW_{\text{rest}}(\text{C IV})$  of quasars in each magnitude bin. The dashed line shows the fit to the  $EW_{\text{rest}}(\text{C IV})$  with the linear function.

### 2.3. Colors of Quasars

To examine how the color of quasars is affected by the Baldwin effect inferred in Section 2.2, we make simple model spectra for each quasar luminosity following previous works (e.g., Fan 1999; Hunt et al. 2004; Richards et al. 2006; Siana et al. 2008; Ikeda et al. 2011, 2012). Here we assume that the continuum spectral energy distribution (SED) of quasars does not depend on the redshift (see, e.g., Kuhn et al. 2001; Telfer et al. 2002; Yip et al. 2004; Jiang et al. 2006). Because Telfer et al. (2002) show that the continuum SED of radio-quiet quasars is independent of the luminosity, we also assume that the continuum SED of quasars does not depend on the luminosity. We adopt the double power-law continuum ( $f_\nu \propto \nu^{-\alpha_\nu}$ ), showing a spectral break at  $\lambda_{\text{rest}} = 1100 \text{ \AA}$ . The spectral slope at the shorter wavelength side is  $\alpha_\nu = 1.76$  (Telfer et al. 2002) while that at longer wavelength side is  $\alpha_\nu = 0.46$  (Vanden Berk et al. 2001). On this continuum emission, strong emission lines are added by adopting the measured  $EW_{\text{rest}}(\text{C IV})$  given in Table 2 and the typical emission-line flux ratios given in Table 2 of Vanden Berk et al. (2001). Here we include only emission lines whose flux is larger than 0.5% of the  $\text{Ly}\alpha$  flux. We also include the Balmer continuum and the Fe II multiplet emission features by adopting the template give by Kawara et al. (1996). The relative strength of the emission lines to the continuum emission is determined by  $EW_{\text{rest}}(\text{C IV})$  measured in Section 2.2, depending on the quasar absolute magnitude (Table 1). The effects of the intergalactic absorption by the neutral hydrogen are corrected by adopting some extinction models. As for the extinction model, a widely used one is the model of Madau (1995). However, Inoue et al. (2014) recently pointed out that the model of Madau (1995) overestimates the IGM attenuation for  $z \sim 4 - 5$ . Therefore we also use the extinction model proposed recently by Inoue et al. (2014) in addition to the model of Madau (1995) for investigating how the adopted model for the intergalactic absorption affects the quasar colors.

Based on the prepared spectral model, we calculated

the  $g' - r'$ ,  $r' - i'$ , and  $i' - z'$  colors of model quasars with different absolute magnitudes (showing different  $EW$  of emission lines) at redshifts from 2 to 6. Here we use the filter response function of Suprime-Cam (Miyazaki et al. 2002) boarded on the Subaru telescope, because we will compare our results with previous observations using Suprime-Cam in the later sections. The simulated colors of the model quasars for each absolute magnitude are shown in the  $r' - i'$  versus  $g' - r'$  diagram (Figure 3) and the  $i' - z'$  versus  $r' - i'$  diagram (Figure 4). To examine the effect of the adopted IGM absorption model, we show the colors of the model quasar spectra adopting the model of Madau (1995) and those adopting the model of Inoue et al. (2014) separately in those figures. For investigating the effect of adopting different IGM absorption models more evidently, the color tracks for quasars with a specific absolute magnitude ( $-27 \leq M_i[z=2] < -26$ ) but adopting two different IGM absorption models are shown in the 2 two-color diagrams (Figure 5). The quasar selection criteria in these two-color diagrams adopted by Ikeda et al. (2011) and Ikeda et al. (2012) are also shown in Figures 3–5. Specifically, the criteria for selecting quasars at  $z \sim 4$  are

$$r' - i' < 0.42(g' - r') - 0.22, \quad (2)$$

$$g' - r' > 1.0, \quad (3)$$

and the criteria at  $z \sim 5$  are

$$i' - z' < 0.45(r' - i') - 0.24, \quad (4)$$

$$r' - i' > 1.0. \quad (5)$$

Figures 3 and 4 clearly show that quasars with a lower luminosity satisfy more easily the selection criteria than quasars with a higher luminosity, both at  $z \sim 4$  and  $z \sim 5$ . This is mainly because the redshifted  $\text{Ly}\alpha$  emission (whose  $EW$  is larger in lower-luminosity quasars) locates at the wavelength within the  $r'$ -band coverage at  $z \sim 4$  and within the  $i'$ -band coverage at  $z \sim 5$ . This result suggests that previous optical photometric surveys for high-redshift low-luminosity quasars overestimated the quasar number density if a spectral template made from bright quasars (such as the composite spectrum given by Vanden Berk et al. 2001) is used, due to the under estimation of the survey completeness. As for the effect of the adopted IGM absorption model, it is clearly shown in Figures 3–5 (especially in Figure 5) that the separation between the color tracks and the selection boundary in the two-color diagrams is smaller when we adopt the model of Inoue et al. (2014) than the case when we adopt the model of Madau (1995). This suggests that previous high-redshift quasar surveys adopting the IGM absorption model by Madau (1995) underestimate the quasar number density due to the over estimation of the survey completeness. Accordingly, it is interesting to assess how the previous quasar surveys actually overestimated or underestimated the number density of high-redshift quasars quantitatively. Therefore, in the next section, we investigate the effects of the luminosity dependence of the quasar spectral features and also the adopted IGM absorption model on the estimates of the survey completeness.

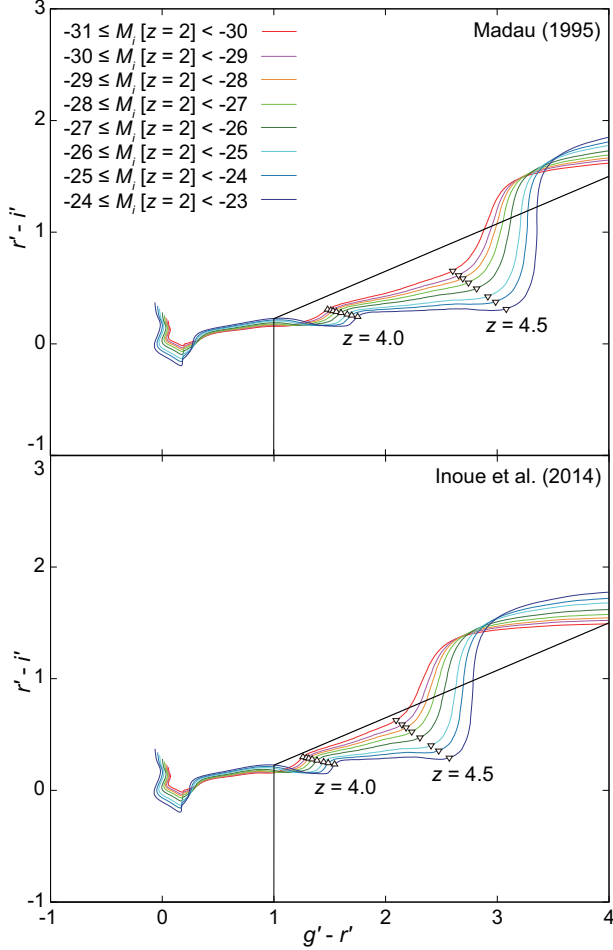


FIG. 3.— Two-color diagram of  $r' - i'$  versus  $g' - r'$ . The color tracks of the model quasar adopting the IGM absorption model of Madau (1995) are shown in the upper panel, while those adopting the model of Inoue et al. (2014) are shown in the lower panel. Different colors denote the different absolute magnitude for each model of the quasar spectrum, as explained in the upper panel. The photometric criteria adopted for selecting photometric quasar candidates at  $z \sim 4$  (Ikeda et al. 2011) are shown by the black solid lines.

### 3. RESULTS

#### 3.1. The COSMOS Data

Here we study how the luminosity dependence of the quasar spectrum and the selection of the IGM absorption model affect the estimate of the survey completeness. For this purpose, we specifically focus on a previous survey for low-luminosity quasars at  $z \sim 4$  and  $z \sim 5$  (Ikeda et al. 2011, 2012). This survey was conducted by using the dataset obtained in the Cosmic Evolution Survey (COSMOS) field. The COSMOS is a treasury program of the Hubble Space Telescope (HST) (Scoville et al. 2007). The COSMOS field covers an area of  $1^\circ.4 \times 1^\circ.4$  which corresponds to  $\sim 2 \text{ deg}^2$ , centered at R.A. (J2000) = 10:00:28.6 and Dec. (J2000) = +02:12:21.0.

For examining the completeness of high-redshift quasar surveys, we use the optical broad-band photometric data in the COSMOS field obtained with Suprime-Cam boarded on the Subaru telescope. In this study we focus on quasars at  $z \sim 4$  and  $z \sim 5$ , that are selected

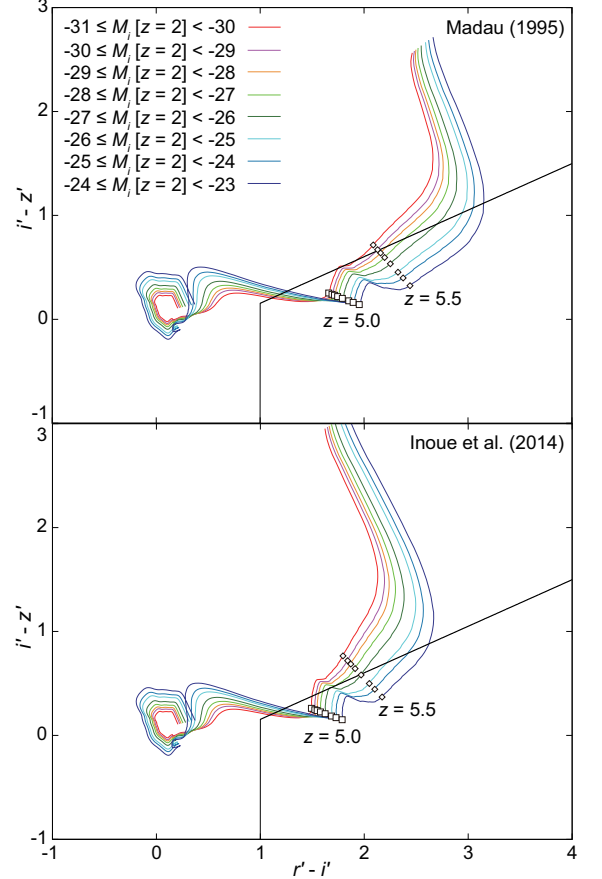


FIG. 4.— Two-color diagram of  $i' - z'$  versus  $r' - i'$ . The color tracks of the model quasar adopting the IGM absorption model of Madau (1995) are shown in the upper panel, while those adopting the model of Inoue et al. (2014) are shown in the lower panel. Colored lines are the same as in Figure 3. The photometric criteria adopted for selecting photometric quasar candidates at  $z \sim 5$  (Ikeda et al. 2012) are shown by the black solid lines.

through  $g'$ -band dropout and  $r'$ -band dropout technique. Therefore we use the Suprime-Cam images obtained with the  $g'$ ,  $r'$ ,  $i'$ , and  $z'$ -band filters (Taniguchi et al. 2007). The  $5\sigma$  depth in  $3''$  aperture magnitudes are  $g' = 26.5$ ,  $r' = 26.6$ ,  $i' = 26.1$ , and  $z' = 25.1$  (Capak et al. 2007).

#### 3.2. Completeness for Quasar Selection

The completeness in quasar surveys is generally defined as the number ratio of the photometrically selected quasars to the existing quasars, as functions of the apparent magnitude and the redshift. We can derive this completeness by simulating the observation through a Monte Carlo approach; i.e., preparing artificially-prepared quasars based on the spectral modeling, putting the simulated quasar into the observational image with photometric errors, detecting them in the same manner as usual object detections, measuring the colors of the detected objects through the forced photometry, applying the quasar selection criteria, and then obtain the completeness by calculating the number ratio of the selected model quasars to the prepared model quasars. In this work, we first estimate the completeness by adopting quasar spectral templates with different emission-line  $EW$ s (that corresponds to different absolute magnitudes as given in Table 1) as a function of redshift, and then

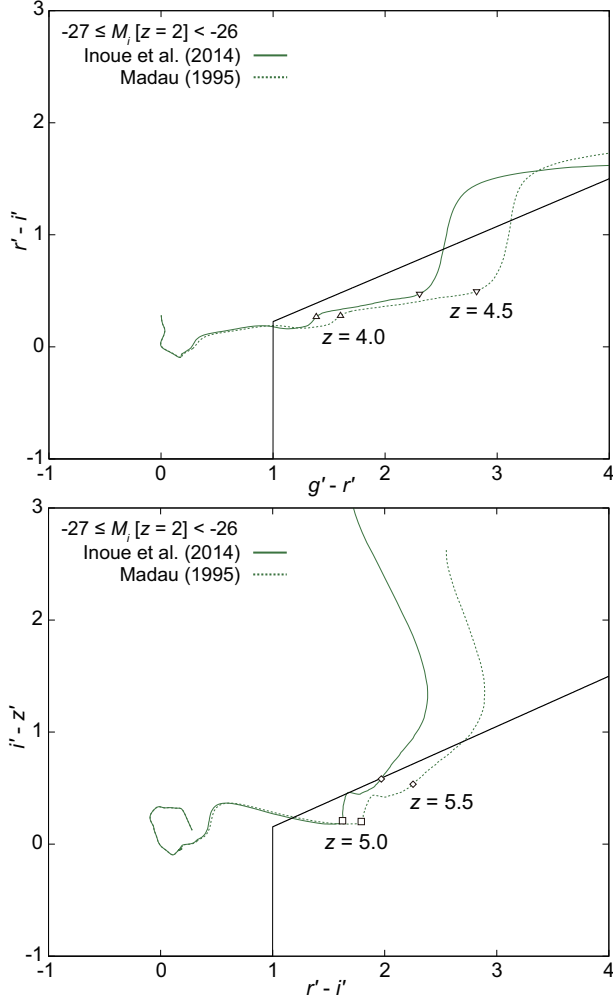


FIG. 5.— Two-color diagrams of  $r' - i'$  versus  $g' - r'$  (upper panel) and  $i' - z'$  versus  $r' - i'$  (lower panel). The solid and dotted lines denote the color tracks of the model quasar with  $-27 \leq M_i[z=2] < -26$ , adopting the IGM absorption model of Inoue et al. (2014) and that of Madau (1995) respectively. The photometric criteria adopted for selecting photometric quasar candidates at  $z \sim 4$  (Ikeda et al. 2011) and  $z \sim 5$  (Ikeda et al. 2012) are shown by the black solid lines in the upper and lower panels, respectively.

we derive the completeness as a function of the apparent  $i$ -band magnitude and redshift.

We generate the model quasar spectra in a similar way as described in Section 2.3. Here we also take into account the intrinsic variation in the continuum slope and  $EW$ s of the emission lines. We assume Gaussian distributions of the power-law slope  $\alpha_\nu$  ( $f_\nu \propto \nu^{-\alpha_\nu}$ ) and C IV  $EW$ s. The mean of the slope is 1.76 at the bluer wavelength than the spectral break at 1100 Å in the rest frame, and 0.46 at the redder wavelength than the break (the same as those in Section 2.3). The standard deviation of the slope is 0.30 at all wavelengths (Fransis 1996; Hunt et al. 2004; Telfer et al. 2002; Ikeda et al. 2011, 2012). We then add emission-line features including the Balmer continuum and Fe II multiplet emission in the same way as described in Section 2.3, taking account of the luminosity dependence of the emission-line  $EW$  (Table 1). Here we also take the intrinsic variation in the emission-line strength into account, whose standard

deviation depends on the quasar luminosity as given in Table 1. In this way we create 1,000 quasar spectra for each composite spectrum at each  $\Delta z = 0.01$  in the redshift range of  $3.4 \leq z \leq 6.0$ . The effects of the intergalactic absorption are corrected by adopting the extinction model of Inoue et al. (2014).

By utilizing the realized spectrum of each model quasar, we calculate  $g'$ ,  $r'$ , and  $z'$ -band apparent magnitudes of the model quasar based on  $i'$ -band apparent magnitude ( $22 \leq i' \leq 24$ ,  $\Delta i' = 0.5$ ). And we derive the colors of each model quasars ( $g' - r'$ ,  $r' - i'$ , and  $i' - z'$ ) in the observed frame. To estimate the photometric completeness, we put the 1000 model quasars for each parameter set (the apparent magnitude with  $\Delta i' = 0.5$ , redshift with  $\Delta z = 0.01$ , and the absolute magnitude of the adopted template with  $\Delta M_i[z=2] = 1.0$ ) into the COSMOS FITS images taken with Suprime-Cam as point sources. For this process, we use the IRAF `mkobjects` task in the `artdata` package. Then we try to detect them in the  $i'$ -band image with SExtractor (Bertin & Arnouts 1996), and measure their colors with the double-image mode. During the process of the source photometry, we correct the photometric offset of each image by referring to Capak et al. (2007).

The measured apparent magnitudes and colors of the simulated quasars are generally different from those before inserted into the Suprime-Cam images, due to the effects of photometric errors and neighboring foreground (or background) objects. Accordingly, some model quasars are not selected as photometric candidates of quasars with the adopted criteria (see Section 2.3), that causes the degrade of the survey completeness. The survey completeness is derived by calculating the fraction of model quasars that are selected as photometric candidates in the above process. Figure 6 shows the derived photometric completeness for quasars with  $i' = 23$  for  $z \sim 4 - 5$ , by adopting different spectral templates with different emission-line  $EW$ s characterized by the  $i$ -band absolute magnitude,  $M_i[z=2]$ . Note that the absolute magnitude defining the spectral template is inconsistent to the combination of the redshift and the assumed apparent magnitude ( $i' = 23$ ); this is because we intend to investigate how the completeness is sensitive to the adopted quasar template (emission-line  $EW$ s) first. The derived completeness highly depends on the adopted spectral template in the sense that the completeness is lower when the spectral template made of higher-luminosity quasars (i.e., with smaller emission-line  $EW$ ) is adopted, even though the same  $i'$ -band apparent magnitude ( $i' = 23$  for Figure 6) is assumed. This is consistent to Figures 3 and 4, where it is inferred that lower-luminosity quasars satisfy the photometric selection criteria more easily. Note that a small dip in the completeness curve is seen at  $z \sim 3.9 - 4.2$  and  $z \sim 5.2 - 5.3$  in Figure 6, that is due to the flux contribution of the C IV emission that makes the  $r' - i'$  and  $i' - z'$  colors redder at each redshift range respectively.

We then derive the completeness as a function of the  $i$ -band apparent magnitude and redshift, by utilizing the results shown in Figure 6. Since the combination of the apparent magnitude and redshift tells us which spectral template (characterized by the  $i$ -band absolute magnitude) should be used for the estimate of the completeness in terms of the absolute magnitude. For this purpose, we

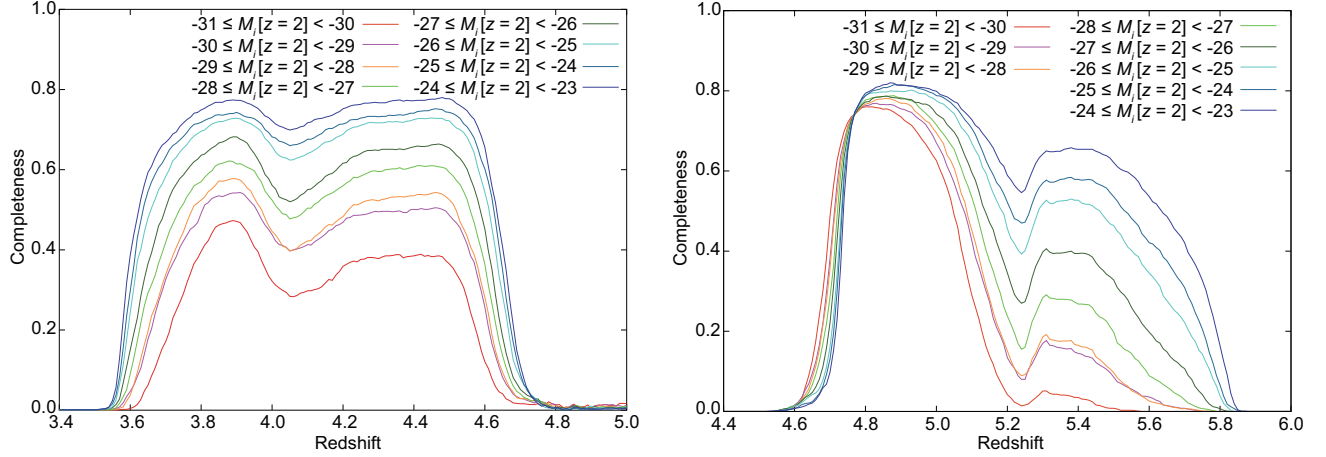


FIG. 6.— The photometric completeness for COSMOS quasars with  $i' = 23$  but having different emission-line  $EW$ s (denoted with different colors) at  $z = 4$  (left) and at  $z = 5$  (right). Note that the absolute magnitude given for each color code is just for characterizing the spectral template but is not related to the signal-to-noise ratio of simulated quasars.

convert the  $i'$ -band apparent magnitude to the absolute AB magnitude at 1450 Å,  $M_{1450}$ , (e.g., Richards et al. 2006; Croom et al. 2009; Glikman et al. 2010) through the following relation:

$$M_{1450} = m_{i'} + 5 - 5 \log d_L(z) + 2.5(1 - \alpha_\nu) \log(1 + z) + 2.5 \alpha_\nu \log\left(\frac{\lambda_{i'}}{1450 \text{ Å}}\right), \quad (6)$$

where  $d_L(z)$ ,  $\alpha_\nu$ , and  $\lambda_{i'}$  are the luminosity distance, spectral index of the quasar continuum ( $f_\nu \propto \nu^{-\alpha_\nu}$ ), and the effective wavelength of the Suprime-Cam  $i'$ -band ( $\lambda_{i'} = 7684 \text{ Å}$ ), respectively. We assume  $\alpha_\nu = 0.46$  in Equation (6). Also we convert  $M_i[z = 2]$  to  $M_{1450}$ , (Richards et al. 2006; Ross et al. 2013) through the following relation:

$$M_i[z = 2] = M_{1450} + 2.5 \alpha_\nu \log\left(\frac{1450 \text{ Å}}{\lambda_{i*}}\right) - 2.5(1 - \alpha_\nu) \log(1 + z), \quad (7)$$

where  $\alpha_\nu$  and  $\lambda_{i*}$  are the spectral index of the quasar continuum (0.46) and the effective wavelength of the SDSS  $i^*$ -band ( $\lambda_{i*} = 7471 \text{ Å}$ ), respectively. Then we derived the completeness for each combination of the redshift and the apparent  $i'$ -band magnitude using an appropriate spectral template characterized by  $M_i[z = 2]$ .

Figure 7 shows the photometric completeness as a function of the redshift and the apparent  $i'$ -band magnitude. Although the derived completeness is generally higher for brighter  $i'$ -band magnitudes as expected, an invert tendency is seen at  $z \gtrsim 5.2$ . This is due to the luminosity dependence of quasar spectrum, that makes the completeness higher for lower-luminosity quasars (see Section 2.3). The estimated completeness at  $z \sim 4$  is generally higher than that estimated by Ikeda et al. (2011), which is also due to the luminosity dependence of quasar spectra since Ikeda et al. (2011) used a composite spectrum of bright SDSS-selected quasars (Vanden Berk et al. 2001) for the completeness estimate. However at  $z \sim 5$ , the estimated completeness in this work is lower than that estimated by Ikeda et al. (2012). This is because the new extinction model (Inoue et al. 2014) makes the completeness lower especially at  $z \sim 5$ , whose effect gives stronger im-

pact on the completeness estimate than the effect of the luminosity dependence of the quasar spectrum.

## 4. DISCUSSION

### 4.1. The QLF at $z \sim 4$

Based on the revised completeness for the previous quasar survey through the optical color selection at the COSMOS field (Ikeda et al. 2011, 2012), we revisit the QLF at  $z \sim 4 - 5$ . First we compute the effective comoving volume of the COSMOS quasar survey as

$$V_{\text{eff}}(m_{i'}) = d\Omega \int_{z=0}^{z=\infty} C(m_{i'}, z) \frac{dV}{dz} dz, \quad (8)$$

where  $d\Omega$  ( $1.64 \text{ deg}^2$ ) is the solid angle of the survey and  $C(m_{i'}, z)$  is the photometric completeness studied in Section 3.2. In Ikeda et al. (2011), eight spectroscopically-confirmed quasars in the COSMOS field are used to derive the QLF at  $z \sim 4$ . Taking into account of the possibility that some of quasar photometric candidates without spectra could also be quasars (that is estimated based on the success rate of the spectroscopic run), we statistically adopt the number of quasars in the COSMOS survey at  $z \sim 4$  as follows; 4.67 for  $-24.09 < M_{1450} < -23.09$  and 6.06 for  $-23.09 < M_{1450} < -22.09$ , respectively (Ikeda et al. 2011). By using these corrected numbers of quasars and the effective comoving volume, we calculate the space density of quasar and their standard deviation as

$$\Phi(m_{i'}, z) = \sum_j \frac{1}{V_{\text{eff}}^j \Delta m_{i'}} = \frac{N_{\text{cor}}}{V_{\text{eff}}}, \quad (9)$$

$$\sigma(\Phi) = \sum_j \left[ \left( \frac{1}{V_{\text{eff}}^j \Delta m_{i'}} \right)^2 \right]^{1/2} = \left[ N_{\text{cor}} \left( \frac{1}{V_{\text{eff}}} \right)^2 \right]^{1/2}, \quad (10)$$

where  $\Delta m_{i'} = 1$ ,  $N_{\text{cor}}$  is the corrected number of quasars. The calculated space density of quasar and their standard deviation are  $(3.49 \pm 1.62) \times 10^{-7} \text{ Mpc}^{-3} \text{ mag}^{-1}$  for  $-24.09 < M_{1450} < -23.09$  and  $(5.24 \pm 2.13) \times 10^{-7} \text{ Mpc}^{-3} \text{ mag}^{-1}$  for  $-23.09 < M_{1450} < -22.09$ , respectively.

The corrected number and calculated space density of  $z \sim 4$  quasars in COSMOS are showed in Table 2, and



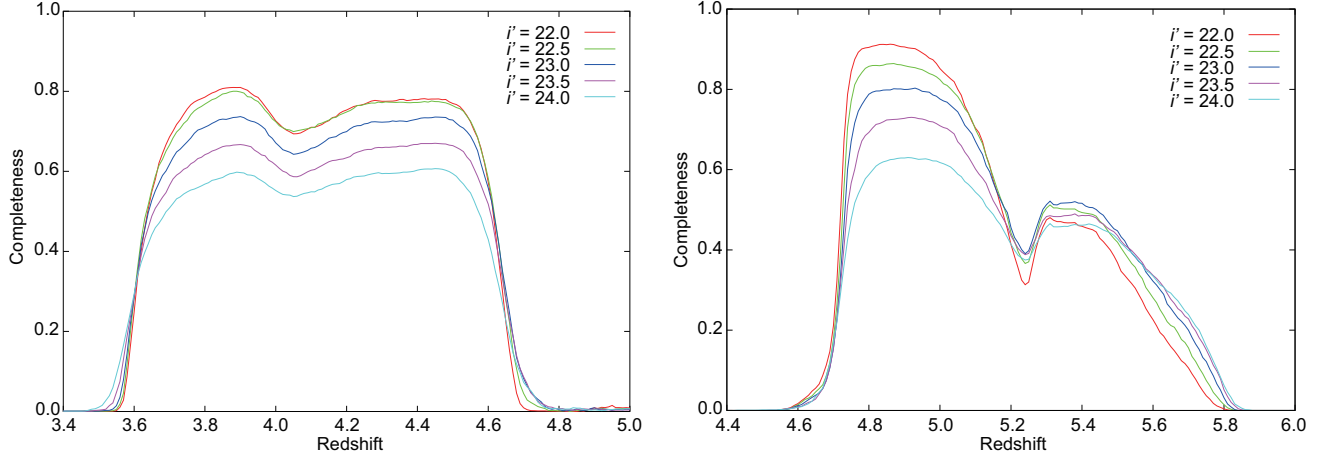


FIG. 7.— The photometric completeness for COSMOS quasars at  $z \sim 4$  (left) and at  $z \sim 5$  (right). Red, green, blue, purple, and cyan lines denote the estimated completeness for quasars with  $i' = 22.0, 22.5, 23.0, 23.5$ , and  $24.0$ , respectively.

the obtained QLF is plotted in Figure 8 with the results of Ikeda et al. (2011) and SDSS (Richards et al. 2006). Although the redshift range of SDSS data ( $4.0 \leq z \leq 4.5$ ; Richards et al. 2006) is slightly different from our study ( $3.7 \leq z \leq 4.7$ ), we apply the weighted least-squares fit to the space density of quasars at  $z \sim 4$  inferred by both our study and SDSS. Here the following double power-law function is adopted:

$$\Phi(M_{1450}, z) = \frac{\Phi(M_{1450}^*)}{10^{0.4(\alpha+1)(M_{1450}-M_{1450}^*)} + 10^{0.4(\beta+1)(M_{1450}-M_{1450}^*)}}, \quad (11)$$

where  $\alpha$ ,  $\beta$ ,  $\Phi(M_{1450}^*)$ , and  $M_{1450}^*$  are the bright-end slope, the faint-end slope, the normalization of the luminosity function, and the characteristic absolute magnitude, respectively (Boyle et al. 2000). Among the four parameters, the bright-end slope is fixed to be  $\alpha = -2.58$  based on the SDSS result at  $z \sim 4$  (Richards et al. 2006). Since the characteristic absolute magnitude becomes too bright when the parameter is treated as a free parameter in the fit, the characteristic magnitude is fixed to be  $M_{1450}^* = -24.4$  based on the result of the COSMOS QLF at  $z \sim 4$  (Ikeda et al. 2011). The best-fit values and  $1\sigma$  standard deviations of  $\Phi(M_{1450}^*)$  and  $\beta$  are  $\Phi(M_{1450}^*) = (3.03 \pm 0.24) \times 10^{-7} \text{ Mpc}^{-3} \text{ mag}^{-1}$  and  $\beta = -1.46^{+0.23}_{-0.19}$ , respectively. These best-fit results are showed in Table 3, and the fitting results are shown in Figure 8. Comparing with the results by Ikeda et al. (2011), we find that our results taking account of the Baldwin effect and the IGM model show  $\sim 24\%$  lower number density at  $z \sim 4$ . This is attributed by the revision of the completeness estimate and the adopted latest IGM absorption model from the previous work (Ikeda et al. 2011). Note that the revised number density of low-luminosity quasars at  $z \sim 4$  is consistent with the number density inferred by recent X-ray observations (Marchesi et al. 2016).

#### 4.2. The QLF at $z \sim 5$

The low-luminosity quasar survey in the COSMOS field found no spectroscopically-confirmed quasars at  $z \sim 5$  in the magnitude range of  $22 < i' < 24$ , and consequently the upper limit on the quasar number density was obtained (Ikeda et al. 2012). Here we investigate how the inferred upper limit is revised when our new

TABLE 2  
THE QUASAR SPACE DENSITY AT  $z \sim 4$  AND THEIR STANDARD DEVIATION

$M_{1450}$ [mag]	$N_{\text{cor}}^a$	This Work $\Phi$ [ $10^{-7} \text{ Mpc}^{-3} \text{ mag}^{-1}$ ]	Ikeda et al. (2011) $\Phi$ [ $10^{-7} \text{ Mpc}^{-3} \text{ mag}^{-1}$ ]
-23.59	4.67	$3.49 \pm 1.62$	$4.35 \pm 2.01$
-22.59	6.06	$5.24 \pm 2.13$	$7.32 \pm 2.97$

<sup>a</sup>  $N_{\text{cor}}$  is the corrected number of the quasars (Ikeda et al. 2011).

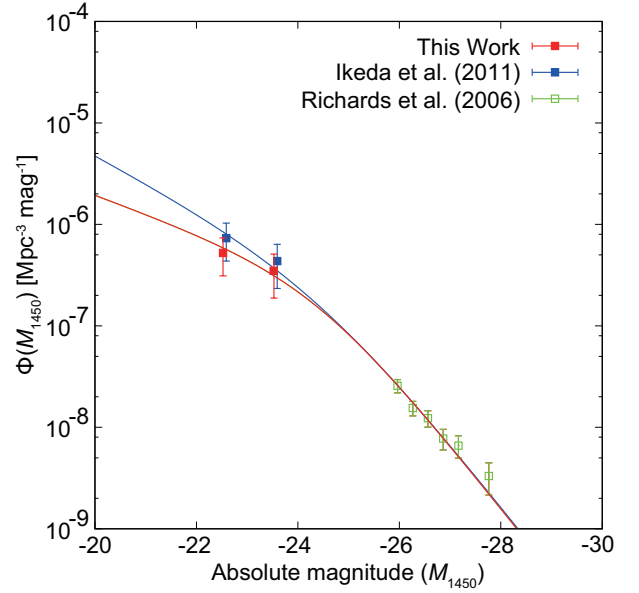


FIG. 8.— The QLF at  $z \sim 4$  derived from the COSMOS data. The red and blue squares are the quasar number density calculated in this work and in Ikeda et al. (2011), respectively. The red squares are slightly shifted to the left direction to avoid the overlap with the blue squares. Green squares are the SDSS results (Richards et al. 2006). The red line shows the fit to our results and the SDSS data, while the blue line shows the fit to the result of Ikeda et al. (2011) and of the SDSS.

completeness estimates are used. We calculate the revised effective comoving volume of the COSMOS quasar survey with Equation (8), based on the new estimates of the survey completeness given in Section 3.2. By



TABLE 3  
BEST-FIT QLF PARAMETERS FOR QUASARS AT  $z \sim 4$

	$\beta$	$\Phi(M_{1450}^*)$ [ $10^{-7} \text{ Mpc}^{-3} \text{ mag}^{-1}$ ]	$M_{1450}^*$ [mag]
This Work	$-1.46^{+0.23}_{-0.19}$	$3.03 \pm 0.24$	$-24.4$ (fixed)
Ikeda et al. (2011)	$-1.67^{+0.11}_{-0.17}$	$3.20 \pm 0.24$	$-24.4 \pm 0.06$

NOTE. — The bright-end slope ( $\alpha$ ) is fixed to be  $-2.58$  in both fits.

TABLE 4  
THE QUASAR SPACE DENSITY AT  $z \sim 5$

$M_{1450}$ [mag]	This Work $\Phi$ [ $10^{-7} \text{ Mpc}^{-3} \text{ mag}^{-1}$ ]	Ikeda et al. (2012) $\Phi$ [ $10^{-7} \text{ Mpc}^{-3} \text{ mag}^{-1}$ ]
$-24.02$	$< 2.00$	$< 1.33$
$-23.02$	$< 3.89$	$< 2.88$

adopting the newly derived effective comoving volume and the statistics of Gehrels (1986), the derived  $1\sigma$  confidence upper limits on the space density of quasars are  $\Phi < 2.00 \times 10^{-7} \text{ Mpc}^{-3} \text{ mag}^{-1}$  for  $-24.52 < M_{1450} < -23.52$  and  $\Phi < 3.89 \times 10^{-7} \text{ Mpc}^{-3} \text{ mag}^{-1}$  for  $-23.52 < M_{1450} < -22.52$  (Table 4). Although no low-luminosity quasar was clearly identified in the FOCAS spectroscopic observation by Ikeda et al. (2012), here we take into account for possibilities that an object whose FOCAS spectra looks a type-2 AGN at  $z = 5.07$  (but with a low significance) and an object without FOCAS spectrum could be quasars at  $z \sim 5$  (see Ikeda et al. 2012 for more details). These results are plotted in Figure 9 with the previous estimates by Ikeda et al. (2012) and also the SDSS results Richards et al. (2006). The new results at  $z \sim 5$ , taking into account of the Baldwin effect and the IGM model, show  $\sim 43\%$  higher number densities than the number density reported by Ikeda et al. (2012), due to the smaller revised completeness at  $z \sim 5$  (Section 3.2) than the completeness given in Ikeda et al. (2012).

#### 4.3. The Redshift Evolution of Quasar Space Density

Here we discuss how the redshift evolution of the quasar number density depends on the quasar luminosity (i.e., the LDDE), based on the revisited completeness and consequent QLF at  $z \sim 4$  and 5. As described in Section 1, the number density of low-luminosity quasars at high redshifts is the key to interpret the LDDE of quasars and to discuss the cosmological evolution of SMBHs for different masses. Figure 10 shows the quasar space density at the different absolute magnitude as a function of redshift. At  $z < 4$ , the quasar space density reported by the 2dFSDSS LRG and Quasar Survey (2SLAQ; Croom et al. 2009), the Spitzer Wide-area Infrared Extragalactic Legacy Survey (SWIRE; Siana et al. 2008), and SDSS (Richards et al. 2006) are plotted. The data at  $z < 4$  is totally consistent with the AGN downsizing evolutionary picture, as pointed out in some earlier works (Croom et al. 2009). On the other hand, various results of the low-luminosity quasar space density are suggested at  $z > 3$ . The result of our study and Ikeda et al. (2011, 2012) which used the COSMOS field suggest that the low-luminosity quasar space density de-

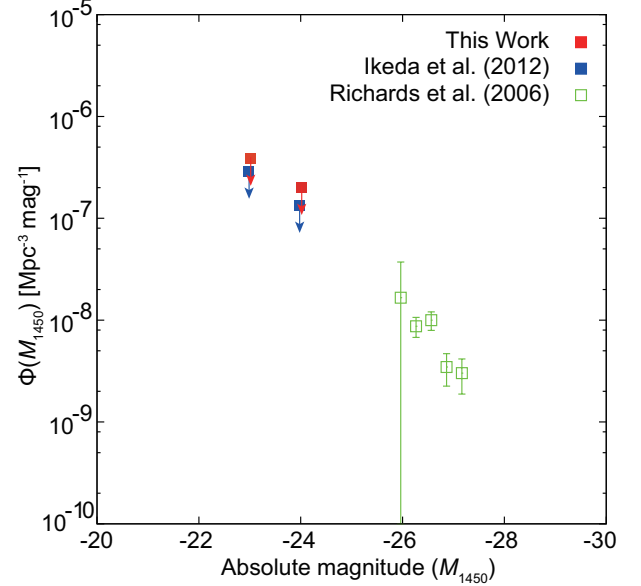


FIG. 9.— Same as Figure 8 but for  $z \sim 5$ . Here the number densities of COSMOS quasars are given as  $1\sigma$  upper limits. The red and blue squares are the upper limits of the quasar number density calculated in this work and in Ikeda et al. (2012), respectively. Green squares are the SDSS results (Richards et al. 2006). The blue squares are slightly shifted to the left direction for clarity.

crease from  $z \sim 2$  to  $z \sim 5$ . This trend is suggested also by recent X-ray surveys of high- $z$  low-luminosity quasars (Marchesi et al. 2016), not only by previous X-ray surveys of relatively bright quasars (e.g., Ueda et al. 2003; Hasinger et al. 2005). However the result of the NOAO Deep Wide-Field Survey (NDWFS) and the Deep Lens Survey (DLS) by Glikman et al. (2011) suggest constant or higher number densities of low-luminosity quasars at  $z \sim 4$  than that at  $z \sim 2 - 3$ . At  $z \sim 6$ , recent studies (e.g., Willott et al. 2010; Kashikawa et al. 2015) suggested lower number density of quasar than our upper limits of them at  $z \sim 5$ . Our result shows that the evolution of low-luminosity quasar number density at  $z \sim 4 - 5$  is consistent with the AGN downsizing, even if we take into account of the Baldwin effect and the latest extinction model of Inoue et al. (2014) for intergalactic absorption in the estimation of the photometric completeness. However, the suggested number density of low-luminosity quasars at  $z \sim 4$  differs between the COSMOS field and the DLS/NDWFS fields. One possible reason for this discrepancy is the criterion of the point-source selection, that is not discussed in our work. Specifically, the DLS/NDWFS survey defines the point source based on ground-based  $R$ -band images (see Figure 4 in Glikman et al. 2010), while the COSMOS sur-

vey defines the point source based on the HST images (Ikeda et al. 2011). Another possible reason for the discrepancy in the number density of high- $z$  low-luminosity quasars in previous surveys is the small sample size of their spectroscopically-confirmed quasars. To clarify the reason for this difference and understand the evolution of the quasar number density more accurately, further observations of low-luminosity quasars in a wider survey area are crucial.

As shown in Sections 4.1 and 4.2, the inferred number density of high-redshift low-luminosity quasars was overestimated or underestimated by a factor of  $\sim 20 - 50\%$  compared with the result of Ikeda et al. (2011, 2012), depending on their redshift and luminosity. This suggests that there was a systematic error caused by the adopted IGM extinction model and the luminosity dependence of quasar spectral template (i.e., the Baldwin effect) in the quasar number density reported in the previous surveys. Note that this systematic error is not seriously large if it is compared with the statistical error in the COSMOS works (Ikeda et al. 2011, 2012), because of the small number of photometric and spectroscopic sample of high- $z$  low-luminosity quasars. However, near-future surveys of high- $z$  low-luminosity quasars such as Subaru/Hyper Suprime-Cam (Miyazaki et al. 2012, see also Matsuoka et al. 2016) and Subaru/Prime Focus Spectrograph (Takada et al. 2014) will observe a numerous number of high- $z$  low-luminosity quasars. In those surveys, systematic errors with a factor of  $\sim 20 - 50\%$  is not negligible at all given their small statistical error. Therefore, understanding the proper method to infer the survey completeness and effective volume as investigated in this work is crucial.

## 5. SUMMARY

In order to derive the high- $z$  low-luminosity QLF accurately, we quantify the influence of the Baldwin effect and the IGM absorption model on the quasar color. We then reevaluate the photometric completeness of low-luminosity quasar surveys with COSMOS images. The main results of this study are as follows.

1. At  $z \sim 4 - 5$ , lower-luminosity quasars are more easily selected by color selection criteria than higher-luminosity quasars when the effects of the Baldwin effect are properly considered.
2. By comparing the quasar model spectra adopting the extinction model by Inoue et al. (2014) with the other model by Madau (1995), we find that the former (latest) model predicts a smaller Lyman-break feature at  $z \sim 4 - 5$ , that makes the color selection of quasars more challenging.
3. The revised completeness is larger at  $z \sim 4$  but smaller at  $z \sim 5$  than our previous works (Ikeda et al. 2011, 2012), due to the effects of the Baldwin effect and IGM model.
4. The revaluated quasar space densities at  $z \sim 4$  are  $(3.49 \pm 1.62) \times 10^{-7} \text{ Mpc}^{-3} \text{ mag}^{-1}$  for  $-24.09 < M_{1450} < -23.09$  and  $(5.24 \pm 2.13) \times 10^{-7} \text{ Mpc}^{-3} \text{ mag}^{-1}$  for  $-23.09 < M_{1450} < -22.09$ , respectively. These densities are lower than the results

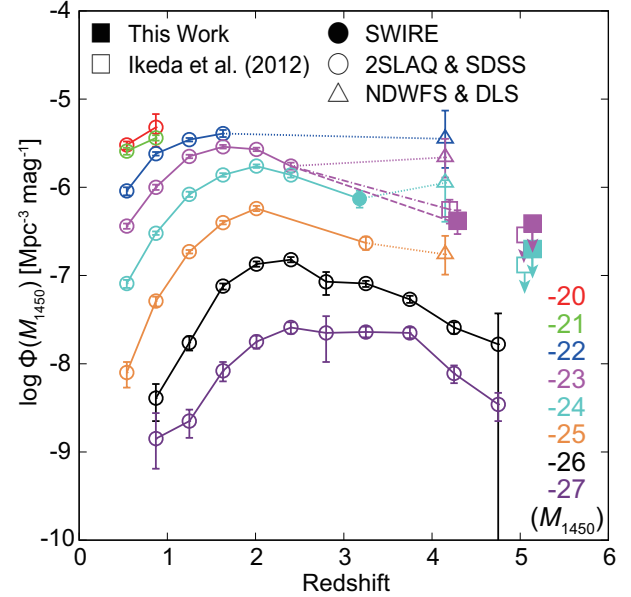


FIG. 10.— Redshift evolution of the quasar space density. Red, green, blue, magenta, light blue, orange, black, and purple lines are the space density of quasars with  $M_{1450} = -20, -21, -22, -23, -24, -25, -26$ , and  $-27$ , respectively. Filled squares and open squares show the results of this study and those of Ikeda et al. (2011, 2012), respectively, in the COSMOS field. Open circles, filled circle, and open triangles denote the results obtained in the 2dFSDSS LRG and Quasar Survey (2SLAQ; Croom et al. 2009), SDSS (Richards et al. 2006), the Spitzer Wide-area Infrared Extragalactic Legacy Survey (SWIRE; Siana et al. 2008), and the NOAO Deep Wide-Field Survey (NDWFS) and the Deep Lens Survey (DLS) by Glikman et al. (2011), respectively. The filled squares at  $z \sim 4$  and  $5$  are slightly shifted to the right direction to avoid the overlap with other symbols.

without considering the Baldwin effect (Ikeda et al. 2011). Therefore the revaluated faint-end slope of our QLF,  $\beta = -1.46^{+0.23}_{-0.19}$ , is flatter than that of Ikeda et al. (2011).

5. The upper limits of the quasar space density at  $z \sim 5$  are  $\Phi < 2.00 \times 10^{-7} \text{ Mpc}^{-3} \text{ mag}^{-1}$  for  $-24.52 < M_{1450} < -23.52$  and  $\Phi < 3.89 \times 10^{-7} \text{ Mpc}^{-3} \text{ mag}^{-1}$  for  $-23.52 < M_{1450} < -22.52$ . These densities are higher than the results without considering the Baldwin effect.
6. Even by taking account of the revisions in the completeness estimate, the inferred luminosity-dependent density evolution of quasars is consistent with the AGN down-sizing evolutionary picture.

We would like to thank Masaru Kajisawa, Masayuki Akiyama, and Kazuyuki Ogura for their helpful comments and suggestions. This work was financially supported in part by JSPS (TN: 25707010, 16H01101, and 16H03958; YT: 23244031 and 16H02166) and also by the JGC-S Scholarship Foundation. We thank the Subaru staff for their invaluable help for obtaining the COSMOS imaging data and spectroscopic follow-up data, and also all members of the COSMOS team. We would also like to thank an anonymous referee for her/his useful comments and suggestions. Data analysis were in part carried out on common use data analysis computer

TABLE 5  
THE NUMBER OF QUASAR SPECTRA FOR MAKING COMPOSITE SPECTRA

	$2.00 \leq z < 2.25$	$2.25 \leq z < 2.50$	$2.50 \leq z < 2.75$	$2.75 \leq z < 3.00$	$3.00 \leq z < 3.25$	$3.25 \leq z < 3.50$
$-31 \leq M_i^a < -30$	0	0	0	4	1	0
$-30 \leq M_i < -29$	7	7	6	13	7	10
$-29 \leq M_i < -28$	94	154	132	124	129	115
$-28 \leq M_i < -27$	438	1181	978	727	738	526
$-27 \leq M_i < -26$	1655	4421	3060	1895	1713	833
$-26 \leq M_i < -25$	3344	7230	3964	1852	1003	266
$-25 \leq M_i < -24$	1651	2534	746	174	25	1
$-24 \leq M_i < -23$	44	16	1	1	0	1
	$3.50 \leq z < 3.75$	$3.75 \leq z < 4.00$	$4.00 \leq z < 4.25$	$4.25 \leq z < 4.50$	$4.50 \leq z < 4.75$	$4.75 \leq z < 5.00$
$-31 \leq M_i < -30$	0	0	0	0	0	0
$-30 \leq M_i < -29$	5	9	9	8	2	1
$-29 \leq M_i < -28$	91	81	57	34	23	13
$-28 \leq M_i < -27$	350	296	132	57	34	22
$-27 \leq M_i < -26$	466	282	75	18	4	2
$-26 \leq M_i < -25$	46	13	1	0	0	0
$-25 \leq M_i < -24$	0	0	0	0	0	0
$-24 \leq M_i < -23$	1	0	0	0	0	0

<sup>a</sup>  $M_i$  denotes  $M_i[z = 2]$ .

system at the Astronomy Data Center, ADC, of the National Astronomical Observatory of Japan. Funding for SDSS-III has been provided by the Alfred P. Sloan Foundation, the Participating Institutions, the National Science Foundation, and the U.S. Department of Energy Office of Science. The SDSS-III web site is <http://www.sdss3.org/>. SDSS-III is managed by the Astrophysical Research Consortium for the Participating Institutions of the SDSS-III Collaboration including the University of Arizona, the Brazilian Participation Group, Brookhaven National Laboratory, Carnegie Mellon University, University of Florida, the French Participation Group, the German Participation Group, Harvard University, the Instituto de Astrofísica de Canarias, the

Michigan State/Notre Dame/JINA Participation Group, Johns Hopkins University, Lawrence Berkeley National Laboratory, Max Planck Institute for Astrophysics, Max Planck Institute for Extraterrestrial Physics, New Mexico State University, New York University, Ohio State University, Pennsylvania State University, University of Portsmouth, Princeton University, the Spanish Participation Group, University of Tokyo, University of Utah, Vanderbilt University, University of Virginia, University of Washington, and Yale University. IRAF is distributed by the National Optical Astronomy Observatory, which is operated by the Association of Universities for Research in Astronomy (AURA) under a cooperative agreement with the National Science Foundation.

## APPENDIX

### DEPENDENCE OF $EW(\text{C IV})$ ON THE QUASAR LUMINOSITY AND REDSHIFT

In Section 2.2, we described that  $EW(\text{C IV})$  of the quasar spectrum does not depend on redshift. To clarify this statement, we make composite spectra for each luminosity and redshift bin. We first divide the 43,953 quasar spectra selected from the BOSS quasar catalog for each  $\Delta M_i[z = 2] = 1$  and  $\Delta z = 0.25$  bin. The number of quasars in each bin is showed in Table 5. We make composite spectra for each bin and measure  $EW(\text{C IV})$  of them in the rest frame. The measured  $EW(\text{C IV})$  is summarized in Table 6. In Figure 11, we show the measured  $EW(\text{C IV})$  as a function of redshift (left panel) and luminosity (right panel), respectively. This figure suggests that  $EW(\text{C IV})$  of the quasar spectrum correlates significantly with the luminosity but does not correlate with the redshift.

TABLE 6  
THE  $EW(C\text{ IV})$  [Å] OF COMPOSITE SPECTRA AT REST FRAME

	$2.00 \leq z < 2.25$	$2.25 \leq z < 2.50$	$2.50 \leq z < 2.75$	$2.75 \leq z < 3.00$	$3.00 \leq z < 3.25$	$3.25 \leq z < 3.50$
$-31 < M_i^a < -30$	...	...	...	13.3	29.8	...
$-30 < M_i < -29$	23.4	19.5	14.3	23.2	18.9	23.8
$-29 < M_i < -28$	24.6	23.5	23.5	22.8	24.1	24.6
$-28 < M_i < -27$	27.2	25.5	27.4	28.3	27.9	27.7
$-27 < M_i < -26$	31.3	32.0	33.3	36.5	34.0	34.3
$-26 < M_i < -25$	40.7	41.2	43.2	46.0	42.9	44.3
$-25 < M_i < -24$	50.5	48.1	50.0	50.4	57.1	56.6
$-24 < M_i < -23$	62.8	57.5	48.6	21.1	...	29.1
	$3.50 \leq z < 3.75$	$3.75 \leq z < 4.00$	$4.00 \leq z < 4.25$	$4.25 \leq z < 4.50$	$4.50 \leq z < 4.75$	$4.75 \leq z < 5.00$
$-31 < M_i < -30$	...	...	...	...	...	...
$-30 < M_i < -29$	20.9	29.2	21.8	20.2	19.9	24.3
$-29 < M_i < -28$	23.4	23.9	21.8	26.8	20.3	21.2
$-28 < M_i < -27$	29.0	29.3	29.2	26.0	30.6	26.0
$-27 < M_i < -26$	34.0	35.4	42.4	36.2	15.4	50.3
$-26 < M_i < -25$	38.0	26.9	82.0	...	...	...
$-25 < M_i < -24$	...	...	...	...	...	...
$-24 < M_i < -23$	17.3	...	...	...	...	...

NOTE. — For the case if a bin contains only one quasar, the  $EW(C\text{ IV})$  measured in the individual spectrum of the corresponding quasar is given.

<sup>a</sup>  $M_i$  denotes  $M_i[z = 2]$ .

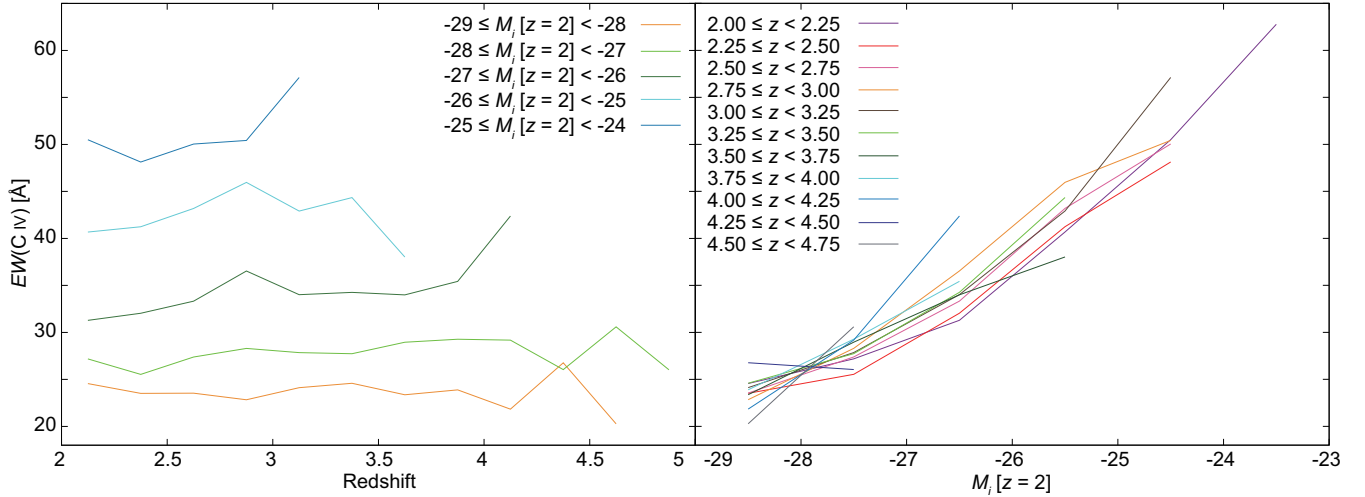


FIG. 11.— The relation between the rest-frame  $EW(C\text{ IV})$  of composite spectra and redshift (left panel) and luminosity (right panel). Only the data made with  $> 20$  quasars are plotted. The line color corresponds to the difference of luminosity (left panel) and difference of redshift (right panel), respectively.

#### REFERENCES

- Ahn, C. P., Alexandroff, R., Allende Prieto, C., et al. 2012, *ApJS*, 203, 21
- Aird, J., Nandra, K., Laird, E. S., et al. 2010, *MNRAS*, 401, 2531
- Baldwin, J. A. 1977, *ApJ*, 214, 679
- Baskin, A., & Laor, A. 2004, *ASPC*, 311, 175
- Bertin, E., & Arnouts, S. 1996, *A&AS*, 117, 393
- Boyle, B. J., Shanks, T., Croom, S. M., et al. 2000, *MNRAS*, 317, 1014
- Capak, P., Aussel, H., Ajiki, M., et al. 2007, *ApJS*, 172, 99
- Cowie, L. L., Songaila, A., Hu, E. M., & Cohen, J. G. 1996, *AJ*, 112, 839
- Croom, S. M., Rhoads, K., Corbett, E. A., et al. 2002, *MNRAS*, 337, 275
- Croom, S. M., Richards, G. T., Shanks, T., et al. 2009, *MNRAS*, 399, 1755
- Dawson, K. S., Schlegel, D. J., Ahn, C. P., et al. 2013, *AJ*, 145, 10
- Dietrich, M., Hamann, F., Shields, J. C., et al. 2002, *ApJ*, 581, 912
- Eisenstein, D. J., Weinberg, D. H., Agol, E., et al. 2011, *AJ*, 142, 72
- Enoki, M., Ishiyama, T., Kobayashi, M. A. R., & Nagashima, M. 2014, *ApJ*, 794, 69
- Fan, X. 1999, *AJ*, 117, 2528
- Fan, X., Strauss, M. A., Richards, G. T., et al. 2006, *AJ*, 131, 1203
- Fontanot, F., De Lucia, G., Monaco, P., Somerville, R. S., & Santini, P. 2009, *MNRAS*, 397, 1776
- Francis, P. J. 1996, *PASA*, 13, 212
- Gehrels, N. 1986, *ApJ*, 303, 336
- Glikman, E., Bogosavljević, M., Djorgovski, S. G., et al. 2010, *ApJ*, 710, 1498
- Glikman, E., Djorgovski, S. G., Stern, D., et al. 2011, *ApJ*, 728, L26
- Gültekin, K., Richstone, D. O., Gebhardt, K., et al. 2009, *ApJ*, 698, 198
- Häring, N., & Rix, H.-W. 2004, *ApJ*, 604, L89
- Hasinger, G., Miyaji, T., & Schmidt, M. 2005, *A&A*, 441, 417
- Hunt, M. P., Steidel, C. C., Adelberger, K. L., & Shapley, A. E. 2004, *ApJ*, 605, 625
- Ikeda, H., Nagao, T., Matsuoka, K., et al. 2011, *ApJ*, 728, L25
- Ikeda, H., Nagao, T., Matsuoka, K., et al. 2012, *ApJ*, 756, 160
- Inoue, A. K., Shimizu, I., Iwata, I., & Tanaka, M. 2014, *MNRAS*, 442, 1805
- Jiang, L., Fan, X., Hines, D. C., et al. 2006, *AJ*, 132, 2127
- Kashikawa, N., Ishizaki, Y., Willott, C. J., et al. 2015, *ApJ*, 798, 28



- Kawara, K., Murayama, T., Taniguchi, Y., & Arimoto, N. 1996, *ApJ*, 470, L85
- Kinney, A. L., Rivolo, A. R., & Koratkar, A. R. 1990, *ApJ*, 357, 338
- Kuhn, O., Elvis, M., Bechtold, J., & Elston, R. 2001, *ApJS*, 136, 225
- Kurk, J. D., Walter, F., Fan, X., et al. 2007, *ApJ*, 669, 32
- Lehmer, B. D., Xue, Y. Q., Brandt, W. N., et al. 2012, *ApJ*, 752, 46
- Madau, P. 1995, *ApJ*, 441, 18
- Marchesi, S., Civano, F., Salvato, M., et al. 2016, *ApJ*, 827, 150
- Marconi, A., & Hunt, L. K. 2003, *ApJ*, 589, L21
- Masters, D., Capak, P., Salvato, M., et al. 2012, *ApJ*, 755, 169
- Matsuoka, K., Nagao, T., Marconi, A., Maiolino, R., & Taniguchi, Y. 2011, *A&A*, 527, A100
- Matsuoka, Y., Onoue, M., Kashikawa, N., et al. 2016, *ApJ*, 828, 26
- Miyaji, T., Hasinger, G., Salvato, M., et al. 2015, *ApJ*, 804, 104
- Miyazaki, S., Komiyama, Y., Sekiguchi, M., et al. 2002, *PASJ*, 54, 833
- Miyazaki, S., Komiyama, Y., Nakaya, H., et al. 2012, *Proc. SPIE*, 8446, 84460Z
- Mortlock, D. J., Warren, S. J., Venemans, B. P., et al. 2011, *Natur*, 474, 616
- Nagao, T., Marconi, A., & Maiolino, R. 2006, *A&A*, 447, 157
- Neistein, E., van den Bosch, F. C., & Dekel, A. 2006, *MNRAS*, 372, 933
- Palanque-Delabrouille, N., Magneville, Ch., Yèche, Ch., et al. 2013, *A&A*, 551, A29
- Pâris, I., Petitjean, P., Aubourg, É., et al. 2012, *A&A*, 548, 66
- Rees, M. J. 1984, *ARA&A*, 22, 471
- Richards, G. T., Strauss, M. A., Fan, X., et al. 2006, *AJ*, 131, 2766
- Ross, N. P., McGreer, I. D., White, M., et al. 2013, *ApJ*, 773, 14
- Scoville, N., Aussel, H., Brusa, M., et al. 2007, *ApJS*, 172, 1
- Shen, Y., & Kelly, B. C. 2012, *ApJ*, 746, 169
- Siana, B., Polletta, M. d. C., Smith, H. E., et al. 2008, *ApJ*, 675, 49
- Smee, S. A., Gunn, J. E., Uomoto, A., et al. 2013, *AJ*, 146, 32
- Takada, M., Ellis, R. S., Chiba, M., et al. 2014, *PASJ*, 66, R1
- Taniguchi, Y., Scoville, N., Murayama, T., et al. 2007, *ApJS*, 172, 9
- Telfer, R. C., Zheng, W., Kriss, G. A., & Davidsen, A. F. 2002, *ApJ*, 565, 773
- Ueda, Y., Akiyama, M., Ohta, K., & Miyaji, T. 2003, *ApJ*, 598, 886
- Ueda, Y., Akiyama, M., Hasinger, G., Miyaji, T., & Watson, M. G. 2014, *ApJ*, 786, 104
- Vanden Berk, D. E., Richards, G. T., Bauer, A., et al. 2001, *AJ*, 122, 549
- Venemans, B. P., Findlay, J. R., Sutherland, W. J., et al. 2013, *ApJ*, 779, 24
- Venemans, B. P., Bañados, E., Decarli, R., et al. 2015, *ApJ*, 801, L11
- Willott, C. J., Delorme, P., Reylé, C., et al. 2010, *AJ*, 139, 906
- Wu, X.-B., Wang, F., Fan, X., et al. 2015, *Nature*, 518, 512
- Yip, C. W., Connolly, A. J., Vanden Berk, D. E., et al. 2004, *AJ*, 128, 2603
- York, D. G., Adelman, J., Anderson, Jr., J. E., et al. 2000, *AJ*, 120, 1579